# Preferential modulation of individual retinal ganglion cells by electrical stimulation

Journal of Neural Engineering

PAPER

# Preferential modulation of individual retinal ganglion cells by electrical stimulation

RECEIVED
5 January 2022

REVISED
20 July 2022

ACCEPTED FOR PUBLICATION
1 August 2022

PUBLISHED
18 August 2022

**Molis Yunzab[1,8,9], Artemio Soto-Breceda[1,2,8], Matias Maturana[1,3,4], Stephanie Kirkby[1,6], Maximilian Slattery[1,6], Anton Newgreen[1,6], Hamish Meffin[1,2], Tatiana Kameneva[2,5], Anthony N Burkitt[2], Michael Ibbotson[1,6] and Wei Tong[1,6,7,*]**

[1] National Vision Research Institute, Australian College of Optometry, Carlton, VIC 3053, Australia
[2] Department of Biomedical Engineering, University of Melbourne, Parkville, VIC 3010, Australia
[3] Department of Medicine, St Vincent's Hospital, University of Melbourne, Parkville, VIC 3010, Australia
[4] Seer Medical, Melbourne, VIC 3000, Australia
[5] School of Science, Engineering, and Computing Technologies, Swinburne University of Technology, Hawthorn, VIC 3122, Australia
[6] Department of Optometry and Vision Science, University of Melbourne, Parkville, VIC 3010, Australia
[7] School of Physics, University of Melbourne, Parkville, VIC 3010, Australia
[8] These authors contributed equally and share first authorship.
[9] Current address: Department of Neurosurgery, Massachusetts General Hospital, Harvard Medical School, Boston, MA, United States Amercia
[*] Author to whom any correspondence should be addressed.

**E-mail:** wei.tong@unimelb.edu.au

**Keywords:** retinal prosthesis, retinal ganglion cells, electrical receptive field, artificial retina, preferential stimulation

Supplementary material for this article is available online

## Abstract

*Objective.* Retinal prostheses have had limited success in vision restoration through electrical stimulation of surviving retinal ganglion cells (RGCs) in the degenerated retina. This is partly due to non-preferential stimulation of all RGCs near a single stimulating electrode, which include cells that conflict in their response properties and their contribution to visiual processing. Our study proposes a stimulation strategy to preferentially stimulate individual RGCs based on their temporal electrical receptive fields (tERFs). *Approach.* We recorded the responses of RGCs using whole-cell patch clamping and demonstrated the stimulation strategy, first using intracellular stimulation, then via extracellular stimulation. *Main results.* We successfully reconstructed the tERFs according to the RGC response to Gaussian white noise current stimulation. The characteristics of the tERFs were extracted and compared based on the morphological and light response types of the cells. By re-delivering stimulation trains that were composed of the tERFs obtained from different cells, we could preferentially stimulate individual RGCs as the cells showed lower activation thresholds to their own tERFs. *Significance.* This proposed stimulation strategy implemented in the next generation of recording and stimulating retinal prostheses may improve the quality of artificial vision.

## 1. Introduction

Retinitis pigmentosa (RP) is an inherited and progressive retinal dystrophy with a prevalence of approximately 1 in 4000 that causes visual impairment and eventual blindness due to loss of photoreceptors [1]. Presently, the most developed clinically available vision restoring treatment for RP is a retinal prosthesis that aims to restore vision via electrical stimulation of surviving retinal neurons [1, 2]. Stimulation is delivered by an electrode array which can be implanted in one of three different locations: on the retinal ganglion cell (RGC) side of the retinal surface (epiretinal), between the photoreceptor layer and the retinal pigment epithelium (subretinal), and between the sclera and the choroid (suprachoroidal).

RGCs are routinely targeted by retinal prostheses. This is because (a) their axons form the optic nerve—natural pathway for the visual stimulus to travel from eye to brain, (b) most RGCs survive after photoreceptor loss [3], and (c) electrical stimulation can activate the RGCs directly or indirectly via other

retinal interneurons [1]. Recent research indicates that there may be more than 30 types of RGCs, each responsible for different aspects of visual information processing [4]. Therefore, selective stimulation of individual RGCs is desired for full restoration of vision [2]. To increase the selectivity of RGC stimulation, researchers have made great advances in fabricating stimulating electrodes with smaller dimensions. However, due to electric field spread, even with electrodes at cellular dimensions <30 $\mu$m, simultaneous stimulation of a patch of RGCs will most likely occur. As a result, stimulation strategies for preferential stimulation of RGCs are under development, but most of them only have very limited targeting capacity, e.g. they may try to preferentially stimulate cells responding to brightness increments (ON-cells), while not stimulating OFF-cells [5–10]. The problem is, there are many different types of ON-cells, with radically different morphologies and functions. It is, therefore, necessary to develop stimulation strategies that can preferentially stimulate a subset of the cells nearby an electrode [11].

White noise stimulation has been previously used as a successful approach for understanding the response of neurons in retina and visual cortex [7, 8, 12–17]. By presenting a series of luminance values obtained randomly from a Gaussian distribution (white noise stimuli) [18], the visual receptive fields can be extracted using spike-triggered average (STA) and spike-triggered covariance (STC) analysis [18]. These visual receptive fields describe the spatial, temporal, or chromatic illumination pattern to which the neurons are most sensitive. In recent years, the same analysis has been adapted to understand the response of neurons to electrical stimulation [7, 8, 12–17]. By delivering electrical stimulation with amplitudes sampled randomly from a Gaussian distribution, both spatial and temporal electrical receptive fields (tERFs) of RGCs have been investigated [7, 8, 12–17].

Previous research, using both epiretinal electrical stimulation [7, 8] and subretinal photovoltaic stimulation [15], has reported the recovery of the tERFs of RGCs. However, the investigation of tERFs has mostly focused on RGC responses to indirect network stimulation [7, 8, 15]. In these studies, they found that ON and OFF RGCs showed distinct features in their tERFs, and the cell-type specific tERFs were likely to be a result of their different signal pathways in the retinal network. Direct RGC stimulation is normally considered the target for epiretinal devices [2]. In terms of sub-retinal devices, it has been previously suggested that the use of direct RGC stimulation could improve the spatial stimulation resolution [19]. Therefore, it is also important to study the tERFs of RGCs in response to direct electrical stimulation.

The implementation of closed-loop systems is revolutionizing the field of neural prosthetics [20–22]. Although existing retinal prosthetics can only deliver electrical pulses for retinal stimulation, the next generation is expected to be capable of both electrical stimulation and recording. By adjusting the stimulation parameters according to the recorded signals, such a closed-loop system will operate at a higher efficacy and restore vision at a higher resolution. This work proposes a stimulation strategy for a closed-loop retinal prosthetic. This stimulation strategy can perform preferential stimulation of individual RGCs using their tERFs, as obtained from direct electrical stimulation. While RGCs are expected to be most sensitive to their own tERFs, none of the previous studies tested the efficacy of tERFs for stimulation. In this work, we demonstrated our proposed stimulation strategy by studying the response preference of individual RGC to stimulation consisting of its own tERFs as well as tERFs obtained from other cells. To record RGC activities, we performed whole-cell patch clamping in explanted rat retinas and subsequent morphological reconstruction and cell type classification. We first studied the responses of RGCs to stimulation delivered intracellularly via the patch clamping electrode, in which the network contribution is negligible. We studied the correlation between the tERFs and their cell types, and assessed the preference of the RGCs to their own tERFs. The results were compared between cells recorded from healthy and degenerated retinas. As existing retinal prosthetics can only deliver electrical stimulation using extracellular electrodes, we also studied the tERFs reconstructed by extracellular stimulation using epiretinal electrodes and demonstrated the potential of our proposed stimulation strategy. While closed-loop retinal prosthetics have not been demonstrated yet, we hope that the technologies will advance soon in this field and the strategy proposed here may benefit their development.

## 2. Methods

All procedures performed in this study were in accordance with the ethics standards of the Animal Care and Ethics Committee of The University of Melbourne (Ethics ID #1814462.3)

### 2.1. Retinal preparation

Data were collected from adult pigmented Long Evans (LE) and Royal College of Surgeons (RCS) rats, of either gender. Specifically, intracellular data were collected from 55 LE rats (2–19 months old), and 37 RCS rats (4–15 months old). Extracellular data were collected from 26 LE rats (2–8 months old). The RCS rats have inherited retinal degeneration and are therefore widely used for research in hereditary retinal dystrophies [23]. In general, RCS rats completely lose their outer nuclear layer as well as RGC light responses 90 days after birth. The retinal preparation was the same as previously described [13]. Briefly, the animals were anesthetized with a mixture of

ketamine (100 mg $kg^{-1}$) and xylazine (10 mg $kg^{-1}$), and then sacrificed after enucleation using intracardiac injection of Letharbarb (1 ml). After enucleation, an incision was made in the cornea, and the retina was dissected in a petri dish filled with carbogenated Ames' solution. The retina was cut into three or four pieces using a razor blade. A single piece of tissue was mounted with RGC side up, on a coverslip and held in place with a stainless-steel harp. The coverslip formed the bottom of a perfusion chamber, which was then placed under an upright microscope for visualization and manipulation. The chamber was continuously perfused with carbogenated Ames' solution at a rate of 3–8 ml $min^{-1}$ at a temperature between 30 °C and 33 °C [14, 24–26].

### 2.2. Whole cell patch clamping

The whole cell current-clamp technique was used to record membrane potentials, as described previously [13]. Briefly, a small hole was first made using a sharp glass pipette in the inner limiting membrane to expose RGCs for recording. A recording pipette with a resistance of 5–10 MΩ was filled with internal solution and mounted on a pipette holder controlled by a motorised micromanipulator. Prior to recording, the pipette resistance was compensated with a bridge balancing circuit on the amplifier. Membrane potential was amplified (BA-1S, NPI), digitised with 16-bit precision at 20 kHz (USB-6221, National Instruments), and stored for offline analysis using a custom-made MATLAB interface (The MathWorks, Inc.). The internal solution was made of 115 mM potassium gluconate, 10 mM HEPES, 2 mM Na-ATP, 0.25 mM Na-GTP, and 250 $\mu$M Alexa Fluor$^{TM}$ 488.

### 2.3. Gaussian white noise stimulation

Gaussian white noise stimulation was delivered to each cell either intracellularly or extracellularly for reconstruction of the tERF. The intracellular stimulation was delivered via the patch clamping pipette. Both the intracellular patch electrode and the return electrode were made of silver and coated with silver chloride before each experiment. The extracellular stimulation was delivered using an electrode made of 100 $\mu$m diameter platinum wire, which was placed in contact with the inner limiting membrane and approximately 50 $\mu$m away from the soma of the cell being patched. The return electrode made of an Ag/AgCl wire was positioned approximately 2.5 mm from the stimulating electrode. For both intracellular and extracellular stimulation, each cell was stimulated with Gaussian white noise for periods of 28 s. The stimulation was repeated until at least 1000 stimulus driven spikes had been detected. The resting time between white noise periods was at least 4 s.

The white noise consisted of trains of currents with random amplitudes sampled from a Gaussian distribution. The amplitude was updated every 150 $\mu$s, with no gap between pulses. The standard deviation of the Gaussian stimulus was adjusted for each cell prior to recording such that each cell produced approximately 1 spike per second. An example of the white noise stimulation current train delivered intracellularly is shown in figures 1(a) and (b) and the cellular response is shown in figures 1(c) and (d).

### 2.4. STC analysis

The tERF was computed using a STC analysis. Spikes were detected using threshold crossings of 0 mV, upon visual validation of the stimulus artifact (figure 1(d)). All detected spikes from all recordings of the single neuron were then assigned to a stimulus matrix (S) with one spike per row. Each row consisted of the stimulus amplitudes preceding the action potentials over a predefined time window (figure 1(c)). The S matrix was made square and symmetrical by S_square = (SS′)/length(stimulus), then the tERFs were computed by calculating the eigenvectors of the S_square matrix.

To ensure the significance of the principal eigenvectors, we only used cells that elicited at least 1000 spikes during all the repetitions of white noise stimulation. Nevertheless, a statistical hypothesis test was performed. The test randomly time-shifts the spike train and repeats the STC analysis on the corresponding randomised spike-triggered stimuli to recover a new set of eigenvalues. For every STC analysis, we ordered their eigenvalues from high to low. If the eigenvalues from the original recording (prior to the random time-shifting) were out of the standard deviation of the eigenvalues obtained from 1000 test repeats, they were considered statistically significant. The significance test for the example cell is shown in figure 1(e). Many cells produced multiple significant eigenvalues. However, only the eigenvector producing the highest eigenvalue was used as the tERF for each cell (figure 1(f)).

### 2.5. Selective stimulation

Following the successful recovery of a RGC's tERF, stimulus trains consisting of all the previously recovered tERFs, including that from the currently patched cell, were injected into the tissues through the same stimulating electrode (figure 2(a), an example from intracellular stimulation). The size of each stimulus train depended on how many tERFs were available at the time of recording, i.e. the $n$th recorded cell would be stimulated with a train consisting of its own tERFs plus the $n-1$ tERFs previously collected. The tERFs in the trains were arranged in random order at a rate of ten tERFs per second, and each of them was scaled by a random positive or negative amplitude (each tERF was scaled once by all the amplitudes), hence the stimulus train included tERFs with upward deflection and downward deflection (figures 2(b) and (c)).

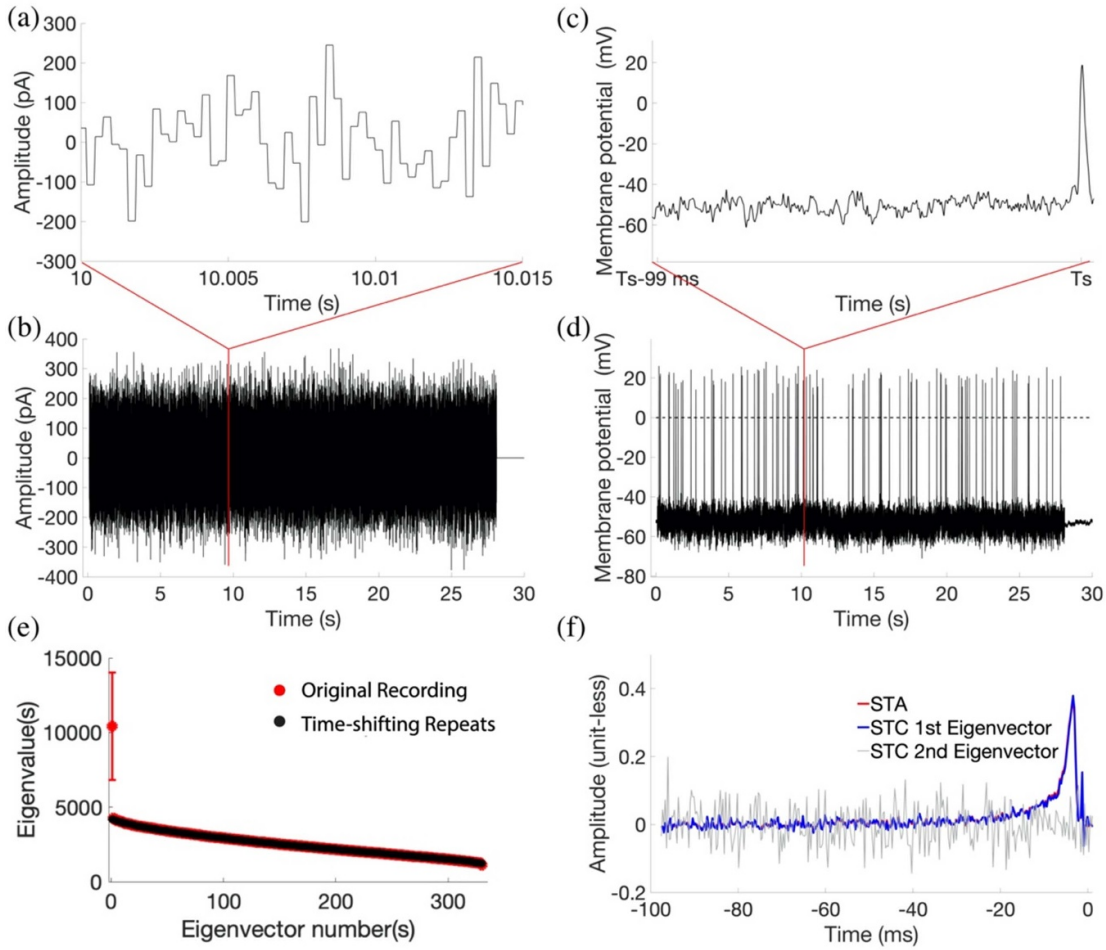


**Figure 1.** Gaussian white noise stimulation protocol and spike-triggered covariance (STC) analysis of an example retinal ganglion cell (RGC). Stimulation was delivered intracellularly via the patch clamping electrode to a cell from a LE rat retina. (a), (b) Example of 28 s of a Gaussian white noise stimulation current train (b). (a) is an enlarged section from b. The amplitude was sampled randomly from a Gaussian distribution; each amplitude was held constant for 150 $\mu$s (a). (c), (d) Example of 30 s of membrane potential recorded during stimulation shown in (b). (d) The dashed line indicates the threshold for spike detection, which was set at 0 mV. The red line marks the section of the recording shown in (c), which shows an example spike and the membrane potential preceding the spike. *Ts* was the time at which the spike occurred. The stimulus between *Ts* and 99 ms before *Ts* (*Ts*—99 ms) was kept as a vector for every spike and sorted into a matrix for the STC analysis. (e) Significance test of the example cell. Every dot is an eigenvalue obtained from the STC analysis ordered from high to low. Red dots represent the eigenvalues of the original recording and black dots represent the eigenvalues after the time-shifting analysis, as described in section 2.4 Error bars represent the standard deviation of the highest eigenvalues from the time-shifting analysis. (f) The spike-triggered average (STA, red line) and the first two eigenvectors (1st eigenvector: blue line; 2nd eigenvector: grey line) from the STC analysis of the example cell. Only the 1st eigenvector of the STC was significant for this cell, which matched the STA.

For each stimulated cell, the efficacy of the response to each tERF was evaluated by fitting a sigmoid function:

$$f(x) = \frac{a}{1 + e^{-b(x-c)}}. \quad (1)$$

In which $f(x)$ is the response probability and $x$ is the amplitude factor. Coefficient $b$ represents scaling factors that determine the saturation amplitudes, $a$ represents the gain of the sigmoidal curves and $c$ represents the thresholds (50% of the saturation level).

To quantify and compare the differences in response thresholds of an individual cell to various tERFs, activation preference was calculated and used for subsequent analysis. Two different activation preferences were calculated. The preference to its own tERF compared to all other tERFs, P(own tERF), was calculated as

$$\mathrm{P(own\ tERF)} = -\frac{\mathrm{Th(own\ tERF)} - \mathrm{Th(all\ other\ tERFs)}}{\mathrm{Th(all\ other\ tERFs)}}. \quad (2)$$

Th(own tERF) is the response threshold (50% of the saturation level) to the tERF of the test cell; Th(all other tERFs) is the average response threshold of the cell to all other tERFs except for its own tERF.

The preference to the tERFs of its own cell type, P(own type), was calculated as

$$\mathrm{P(own\ type)} = -\frac{\mathrm{Th(own\ type)} - \mathrm{Th(all\ other\ types)}}{\mathrm{Th(all\ other\ types)}}. \quad (3)$$

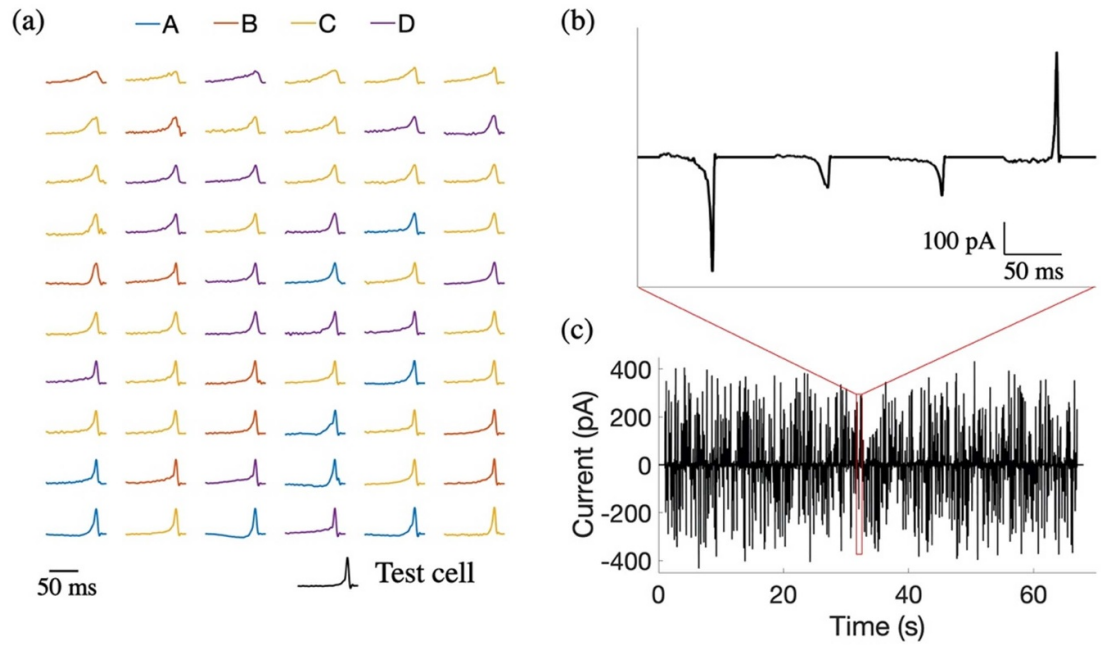


**Figure 2.** Selective stimulation strategy protocol. (a) An example of a tERF stimulation library collected from intracellular stimulation. This library is composed of 60 previously recorded RGC tERFs (coloured) and the tERF of the test RGC (black). All tERFs are arranged in ascending order of peak amplitudes. The morphological types of the RGCs (A, B, C, or D type) to which each tERF belonged to are indicated by the colour of the tERFs. (b), (c) Example of 68 s of stimulation train injected into the test RGC, which contains tERFs from the library scaled by different amplitudes (c). The red line marks the section of the stimulation train shown in b which shows four randomly scaled tERFs. tERFs in the stimulus trains were 50 ms long and were separated by a 50 ms period.

Th(own type) is the average response threshold to all the tERF of the same cell type of the test cell; Th(all other types) is the average response threshold of the cell to all the tERFs of other cell types.

### 2.6. Morphology reconstruction and cell classification

To confirm cell classification, the following technique was used to image the cells and analyse their morphology. During current-clamp, the RGCs were filled with intracellular solution, which contained Alexa Fluor™ 488 dye. Following stimulation and recording of the RGCs, the retinal tissue was infused with Sulforhodamine 101 (red dye). The tissue was subsequently imaged using a confocal microscope and the cell morphology was reconstructed using Image J/Fiji package [27] (figure 3). The cells were classified into different morphological types (type A–D) according to the soma diameter, dendritic field size and structure, and dendritic field stratification (stratification depth, mono- or bistratified), as previously described in detail [13]. In general, A-cells have large soma and dendritic field sizes, while B-cells have small somas and dendritic fields. C-cells tend to display soma and dendritic fields with medium sizes, and bistratified cells are classified as D-cells. Figure 3 shows representative confocal images of example A–D cells. As RGCs in RCS rats had lost their light response, we used the dendritic field stratification depth ($s(x)$) to classify the cells from both RCS and LE rats into different light response types. The stratification depth was quantified as a percentage of the inner plexiform layer (IPL) thickness, according to

$$s(x) = 100\% \times \frac{L_s - L_x}{L_s - L_e}. \quad (4)$$

In which $L_x$ refers to the depth of a terminal dendrite, $L_s$ and $L_e$ represent the ganglion cell layer/IPL (GCL/IPL) border and the IPL/inner nuclear layer (IPL/INL) border, as labelled in figure 3. Cells that stratified in the inner part of the IPL ($s(x) < 40\%$) are denoted as OFF-cells. Cells that stratified in the outer part of the IPL ($s(x) > 40\%$) are referred to as ON-cells. Bistratified cells are ON-OFF cells.

### 2.7. Receptive field analysis

To study the correlation between receptive fields and cell types, we performed K-means cluster analysis [28, 29] using the parameters extracted from the receptive fields, as shown in figure 4. All the tERFs were firstly arranged in a matrix with one tERF per row. The covariance of the resulting tERFs matrix was then calculated and its eigenvectors found. The three eigenvectors with the highest eigenvalue were extracted and labelled as $e1$, $e2$, and $e3$ (figure 4(a)). Each tERF was then projected onto the eigenvectors $e1$, $e2$, and $e3$, resulting in the vectors $v1$, $v2$ and $v3$ (figure 4(b)). These eigenvectors were used for the K-means cluster analysis. To determine the number of clusters $K$ in the

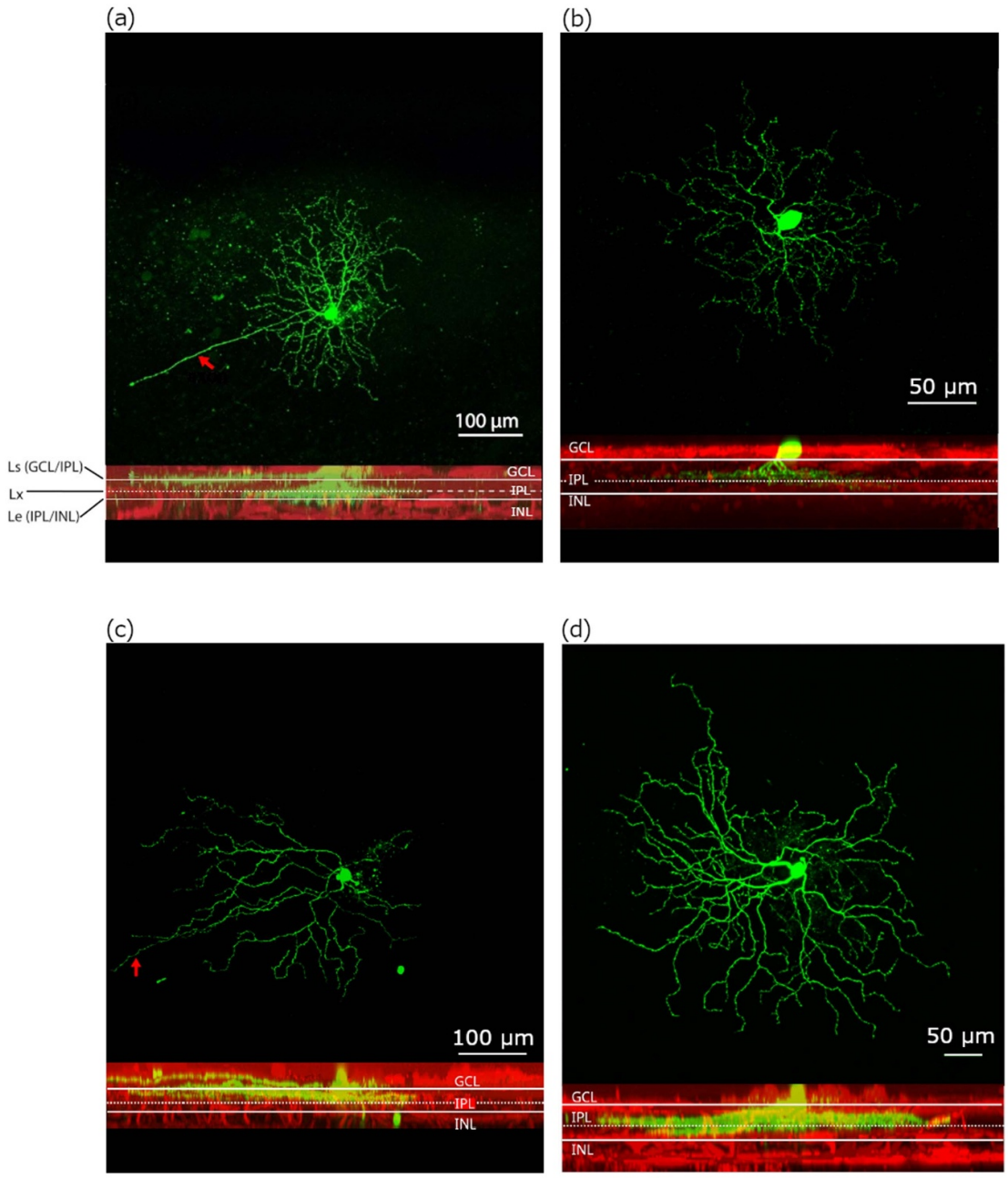


**Figure 3.** 3D morphological reconstruction of a: the example A cell (OFF) shown in figure 1. The cell is filled with Alexa Fluor™ 488 dye. Top: The Z-projection view of the cell from which the soma and dendritic field diameters were measured. Bottom: The lateral view of the cell (green) and the extracellular matrix (red). The interfaces between GCL and IPL, and IPL and INL are marked by horizontal lines. The dashed line corresponding to the stratification of the dendritic tree, which is 30% from the INL (interface between the outer IPL and inner IPL) in the IPL plane. According to the stratification, this is an OFF cell. The morphological type of the cell is determined by the soma and dendritic diameters as well as location of the dendritic stratification. This cell is classified as A cell based on its morphological features. (b) A class B cell (OFF), (c) a class C cell (ON), and (d) a class D cell (ON-OFF). The red arrows in a and c point to the axons of the neurons, the axons of b and d could not be recovered during the reconstruction.

K-means algorithm, the Error Sum of Squares (ESS) was plotted as a function of $K$, as shown in figure 4(c). We considered the 'elbow' for both intracellular and extracellular protocols to be between three and five clusters. We determined that three was the best choice of $K$ for intracellular stimulation and four for extracellular stimulation. This was for several reasons, e.g. with higher $K$ there were clusters with only 1 element. The morphological characteristics, class, and type of light response of the cells were not used as input variables in the cluster classification algorithm, therefore, the clusters do not depend on those parameters.

## 3. Results

### 3.1. tERF from intracellular stimulation

We first reconstructed tERFs according to the responses of RGCs to Gaussian white noise current stimulation. The stimulation was delivered intracellularly via patch-clamp electrodes, in which

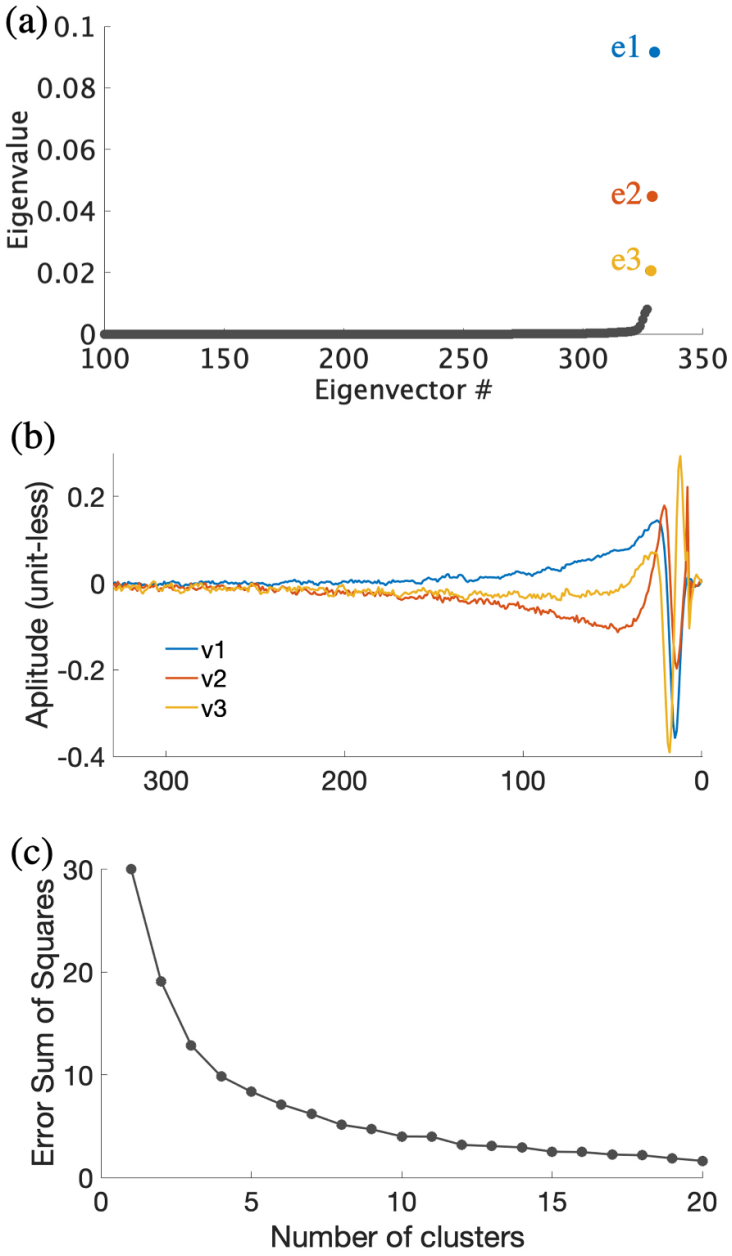


**Figure 4.** Analysis of tERFs obtained from Gaussian white noise stimulation. The analysis shown here is based on the data obtained from intracellular stimulation of LE rat RGCs. (a) Eigenvalues of the covariance matrix containing all tERF waveforms. The three highest eigenvalues are labelled as *e*1, *e*2 and *e*3. (b) The three eigenvectors corresponding to the highest eigenvalues are labelled as *v*1, *v*2 and *v*3. The *y*-axis represents unitless amplitude, and the *x*-axis represents samples. (c) Error sum of squares (SSE) per number of clusters. The 'elbows' of the curve are considered to occur between cluster numbers of 3 and 5. We then determined the optimal number used for K-means clusters to be 3, as the other cluster numbers will lead to clusters with only one element.

**Table 1.** Summary of the number of intracellular tERFs obtained in each morphological type and light response type in both LE and RCS rats.

| | Morphological type | | | | Light response type | | | |
|---|---|---|---|---|---|---|---|---|
| Animal model | A | B | C | D | ON | OFF | ON-OFF | Total |
| LE | 10 | 9 | 27 | 15 | 14 | 31 | 16 | 61 |
| RCS | 9 | 14 | 17 | 5 | 18 | 19 | 8 | 45 |

the retinal network contribution was insignificant. An example of the stimulus and the cell's response are shown in figures 1(a)–(d). A statistical hypothesis test based on an STC analysis revealed that this example cell has a single excitatory receptive field, which is denoted as its tERF in this study (figure 1(f)). We recorded from a total of 61 RGCs from LE rats and 45 RGCs from RCS rats, as summarised in table 1. No

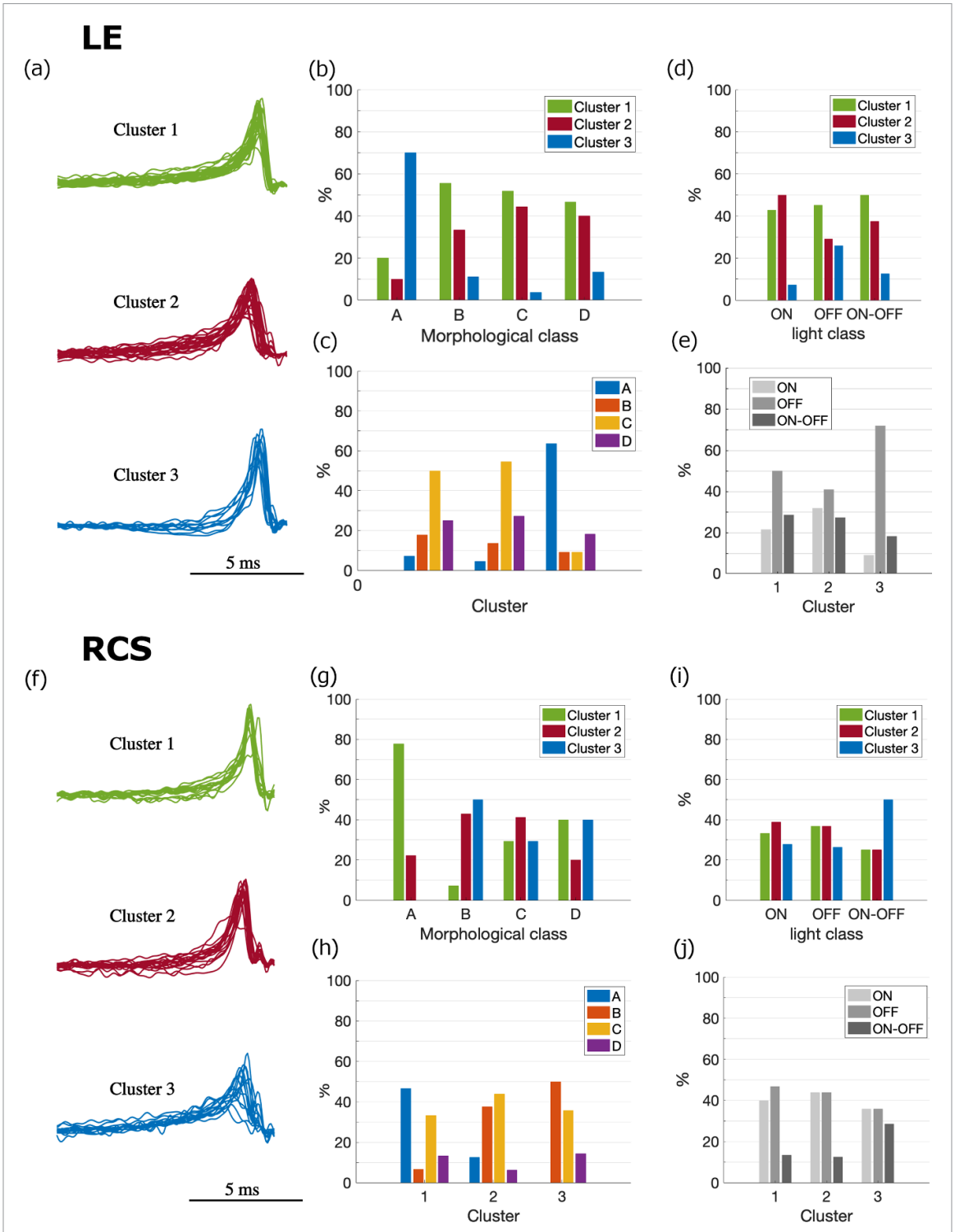


**Figure 5.** Cluster analysis of tERFs obtained from intracellular stimulation of LE (a)–(e) and RCS (f)–(j) rat RGCs. The clustering was based on K-mean analysis using tERF characteristic variables *v1*, *v2* and *v3*, as described in section 2.7 (a), (f) The tERFs grouped by clusters. (b), (g) Distribution of percentage of each cluster in each morphological type. (c), (h) Distribution of percentage of morphological types in each cluster. (d), (i) Distribution of percentage of each cluster in each light response type. (e), (j) Distribution of percentage of light response types in each cluster.

significant suppressive receptive field was observed from any recorded cells. After stimulation and recording, we reconstructed the morphology of every RGC (figure 3), and classified them into different morphological types (A–D), as previously described [13]. All of the recovered tERFs from LE rats after a clustering analysis are shown in figure 5(a). Although these tERFs had varying amplitudes and widths, they all displayed a notable, single upward deflection.

To understand the variability of the tERFs across different cell types, we performed different analysis to study the correlation between the tERFs and the cell types. We first compared the response delays, tERF amplitudes and the time constant tau

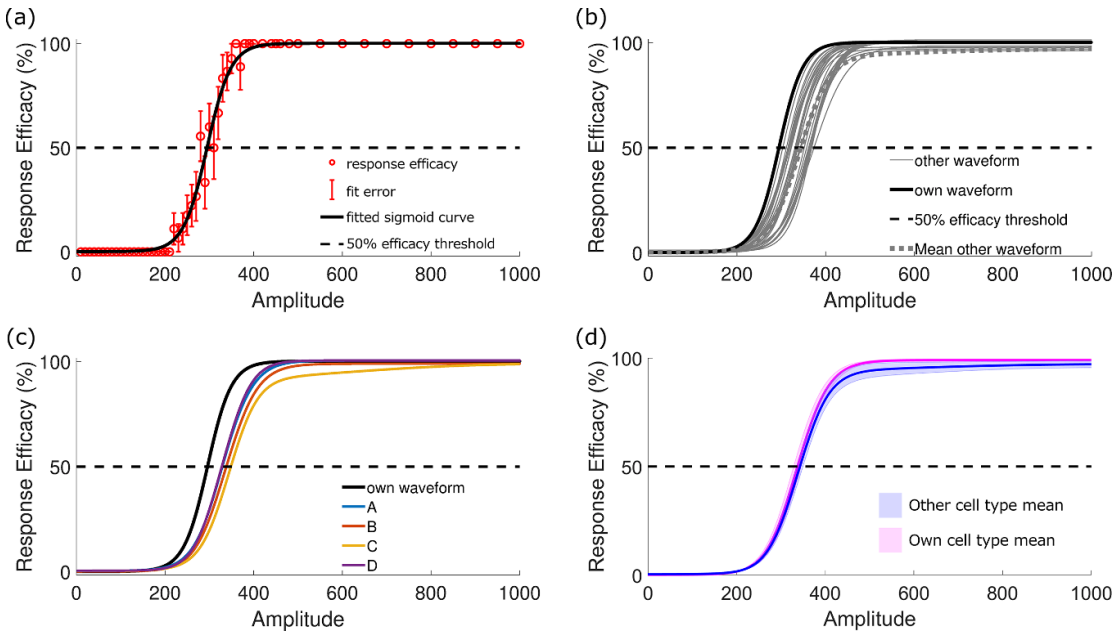


**Figure 6.** Response efficacy analysis for selective stimulation. Data obtained via intracellular stimulation of an example RGC from a LE rat. (a) Example of a sigmoid curve fit (black curve) to the example cell's response (red dot) to a single tERF that has been scaled by various amplitude factors. The efficacy of the response to the tERF can be approximated well by the sigmoid curve. Fit errors are indicated by the error bars. The threshold for response efficacy is set to be efficacy = 50% (black dash line). (b) Each grey curve represents the response efficacy curve to a single tERF in the library used to stimulate the cell. The grey dashed curve represents the average response efficacy curve to all the tERFs in the library. The black curve is the response efficacy curve to the cell's own tERF. (c) Average response efficacy curves to tERFs from cells of different morphological types (coloured curves) and the response efficacy curve to the cell's own tERF (black curve). (d) The average response efficacy curve to tERFs of the cell's own morphological type (magenta curve) and average response efficacy curve to all tERFs of different morphological types to the example cell (other cell type mean, blue curve). Error bars are SEM. This cell is classified as B and OFF ganglion cell based on its morphological features.

across different cell types. No significant difference was found (data not shown). We then performed K-means cluster analysis using the eigenvectors from the tERF matrix, as described in the section 2.7 and figure 4, and three clusters were obtained from LE rats (figure 5(a)). Figures 5(b) and (c) summarize the correlation between these three clusters and the four morphological cell types. A-cells that had large soma sizes and large dendritic field sizes were the most prominent, as over 70% of A-cells were in Cluster 3 (figure 5(c)), while the other morphological cell types included similar percentages of Cluster 1 and 2 cells (figure 5(b)). The percentages of C-cells in both Clusters 1 and 2 were higher than 50%, which was likely due to a larger number of C-cells collected in this study (table 1). Figures 5(d) and (e) show the correlation between the clusters and the light response types. The majority of ON and ON-OFF cells were in Clusters 1 and 2, and OFF cells had three clusters distributed relatively evenly (figure 5(d)). Figure 5(e) indicates that ∼70% of Cluster 3 cells were OFF cells.

The same clustering analysis was also performed with data obtained from RCS rats (figures 5(f)–(j)) and three clusters detected. Similar to the results obtained from LE rats, A-cells were the most prominent as nearly 80% of A-cells were in Cluster 1. The correlation was less obvious between the three clusters and their light response types.

### 3.2. Preferential stimulation using intracellular electrodes

After reconstructing the tERF for each cell, we tested the hypothesis that the cells showed preferential responses to their own receptive fields compared to those from the other cells. To test this hypothesis, we delivered stimulus trains composed of the tERFs obtained from all the cells recorded prior to the test cell as well as the cell's own tERF (figure 2). Figure 6 shows the response efficacy analysis of an example RGC. We fitted the response of the cell to each tERF using a sigmoidal curve (equation (1)) and defined the stimulation threshold as the point where the response efficacy reached 50% (black dash lines). The cell's response to its own tERF (black curve) was then compared to that of all the other tERFs (grey curves), as shown in figure 6(b). This example cell showed the lowest stimulation threshold to its own tERF, as it was the first curve to reach 50% threshold, indicating its preference to its own tERF. For each cell, we also compared their preference to different cell types by comparing the cell's response to its own tERF and an average response efficacy curve to the tERFs from each cell type, as plotted in figure 6(c). This example cell showed lower average thresholds to A- and D-cells than B- and C-cells. Figure 6(d) shows the sigmoidal curve fitting of this example cell's response to all the tERFs from its own cell type, compared to its response

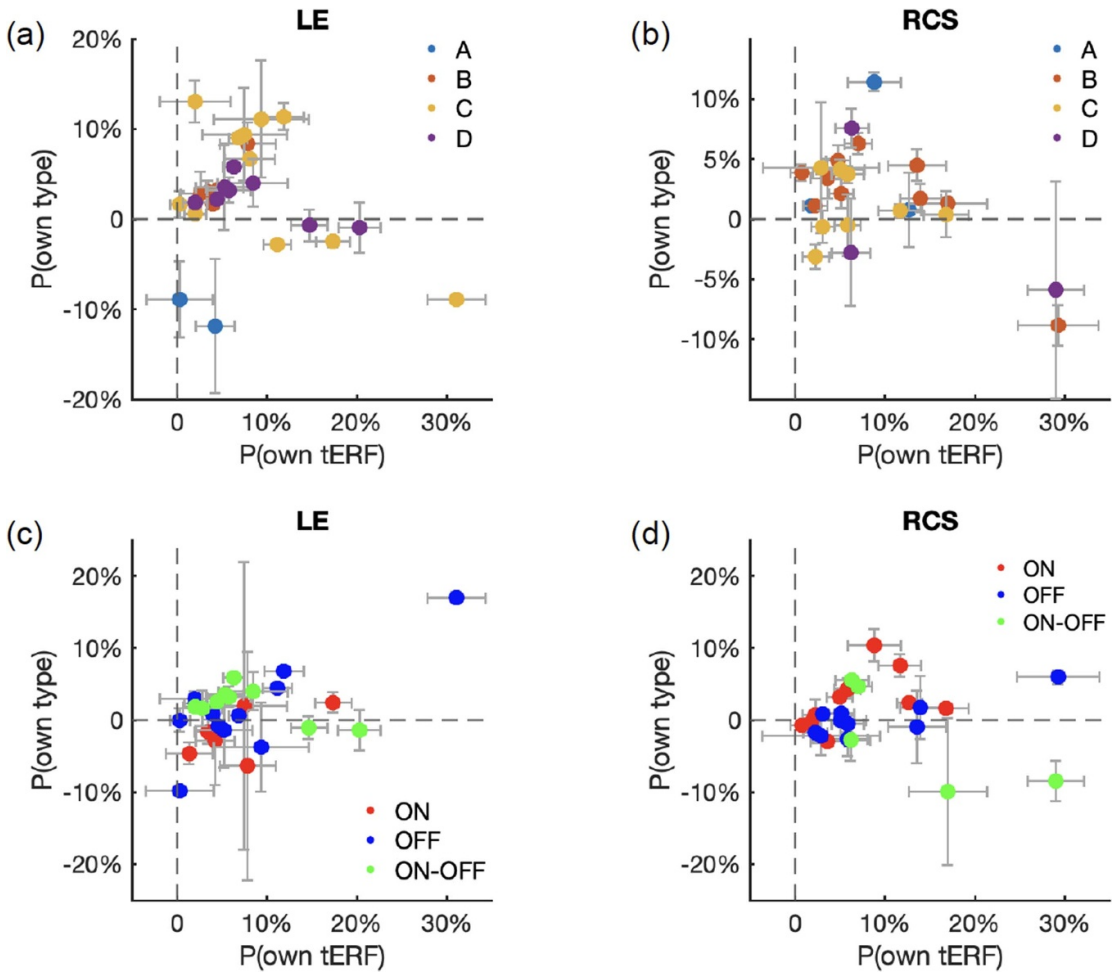


**Figure 7.** Population analysis of activation preference from intracellular stimulation. The analysis is based on RGC morphological types ((a), (b)) and light response types ((c), (d)) for LE rat (a), (c) and RCS rat (b), (d). In each subplot, the activation preference was obtained according to equation (2) or (3). Colours indicate to which cell type (A, B, C and D, or ON, OFF and ON-OFF) each cell belongs. The dashed lines indicate the line of equality. Error bars represent SEM.

to the tERFs of all other cell types; it shows a slightly lower threshold in response to tERFs of its own cell type, as well as a higher efficacy.

To quantitively compare the differences in response thresholds to various tERFs of individual cells, we calculated the activation preference according to equations (2) and (3), as described in section 2.5 The activation preference results are summarised in figure 7. In each scatter plot, a positive $x$ value indicates that the cell could be activated by its own tERF with a lower threshold than other tERFs. The preference increases with the $x$ value. For both LE and RCS data, all cells showed lower threshold to their own tERFs, suggesting the potential of preferentially stimulating individual RGC using their own tERFs. The degree of preference varies across cells, and a point at 20% of P(own tERF) indicates that the threshold to its own tERF is 20% lower than the average of all other cell's tERFs. A positive y value in each scatter plot indicates that the cells could be activated at a lower threshold with the tERFs from its own cell type. The preference increases with the $y$ value. Twenty out of 27 cells (74.1%) recorded from LE rats showed lower thresholds to tERFs from their own morphological types. Nineteen out of 25 cells (76%) from RCS rats showed preference to the tERFs from their own morphological types. Similar results were also found after analysing the response efficacy based on their light response types that 16 out of 27 cells (59.3%) from LE rats and 13 out of 25 cells (52%) from RCS rats tended to show lower thresholds to tERFs from their own cell types. Although the ratios of cells that showed preference to their own cell types were similar between LE and RCS rats, the cell types of the ones that did not show preferences were different between the animal models. For example, most ON cells (4 out of 6) in LE rats (figure 7(c)) did not show preferences to their own cell type, and most of the ON cells (7 out of 10) in RCS rats could be activated by lower thresholds using the tERFs from their own cell type.

### 3.3. tERF from extracellular stimulation

After confirming the effectiveness of using tERF to selectively stimulate individual RGCs intracellularly, we studied their tERFs and the efficacy of the selective

**Table 2.** Summary of the number of extracellular tERFs obtained in each morphological type and light response type in LE rats.

| | Morphological type | | | | Light response type | | | |
|---|---|---|---|---|---|---|---|---|
| Animal model | A | B | C | D | ON | OFF | ON-OFF | Total |
| LE | 14 | 9 | 5 | 7 | 11 | 17 | 7 | 35 |

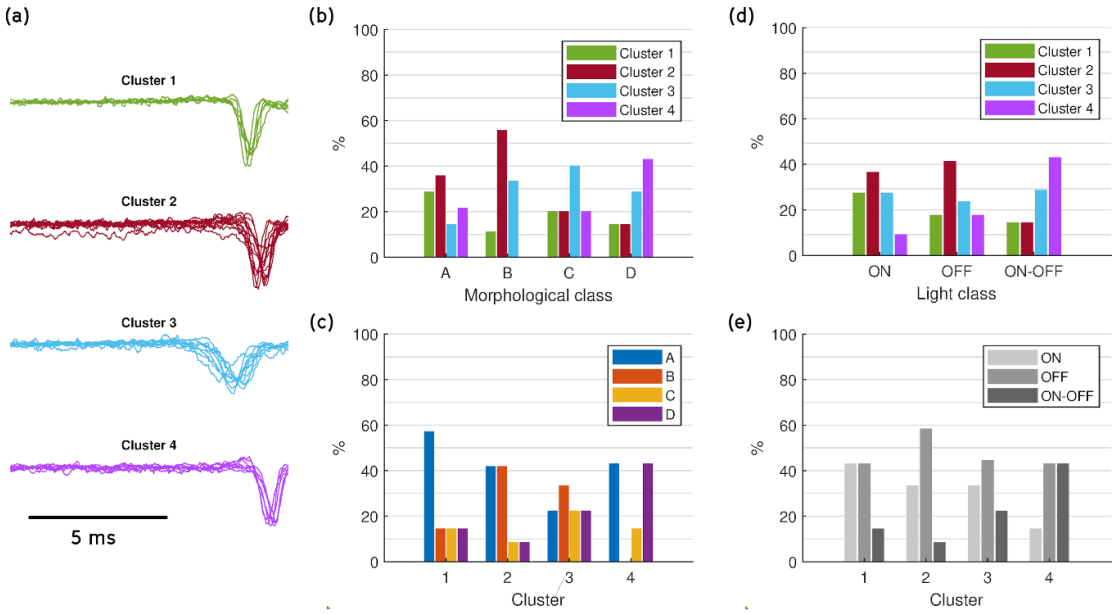


**Figure 8.** Cluster analysis of tERFs obtained from extracellular stimulation of LE rat RGCs. Four clusters were identified based on K-mean analysis using tERF characteristic variables v1, v2 and v3, as described in section 2.7 (a) tERFs grouped by clusters. (b) Distribution of percentage of each cluster in each morphological type. (c) Distribution of percentage of morphological types in each cluster. (d) Distribution of percentage of each cluster in each light response type. (e) Distribution of percentage of light response types in each cluster.

stimulation protocol via extracellular stimulation. In this study, extracellular stimulation was delivered epiretinally via a platinum electrode placed about 50 $\mu$m away from the soma. The responses of the cells were recorded intracellularly via whole-cell patch clamping, as in the previous sections of the paper.

Similar to intracellular stimulation, the STC analysis, together with the significant hypothesis test described in section 2, revealed a single excitatory receptive field according to the RGC response to Gaussian white noise stimulation delivered extracellularly. We were able to reconstruct tERFs from a total of 35 RGCs from LE rats (table 2), and their tERFs were clustered and shown in figure 8(a). All tERFs exhibited a notable, single downward deflection and were more variable in shape compared to the intracellular tERFs. The response delays of all tERFs were within 5 ms, indicating that the responses of RGCs were likely due to direct electrical stimulation, instead of indirect network stimulation [13].

The clustering analysis identified four different clusters from these RGCs (figure 8). B-cells that had small soma and dendritic field sizes were the most prominent, as nearly 60% of them were in Cluster 2 and there were no Cluster 4 cells (figure 8(b)). The other cell types had no clusters that took up over 50% of the cells. According to figure 8(d), Cluster 1 was composed of nearly 60% A-cells. In comparison, Cluster 2 was mostly A- and B-cells, and Cluster 4 was mainly A- and D-cells. Figures 8(c) and (d) summarizes the correlation between the four clusters and the light response types. The clusters were distributed relatively evenly in all light response types (figure 8(c)), with nearly 60% of Cluster 2 cells being OFF cells (figure 8(e)).

### 3.4. Preferential stimulation using extracellular electrodes

We performed the preferential stimulation protocol using the tERFs reconstructed via extracellular stimulation. As a preliminary study, here we tested the protocol using a total of 15 RGCs, which were composed of five A-cells, eight B-cells and two D-cells. These include three ON cells, ten OFF cells and two ON-OFF cells. Figure 9 summarizes the preference of all recorded RGCs to different tERFs according to equations (2) and (3). As expected, all of the cells preferred their own tERFs over the other tERFs, exhibiting lower thresholds when stimulated by their own tERFs (figure 9). When comparing their preference to their own cell type, 10 out of 15 (66.7%) cells preferred their own morphological type (figure 9(a)). Interestingly, all B- and D-cells recorded in this study preferred their own morphological types, but none of

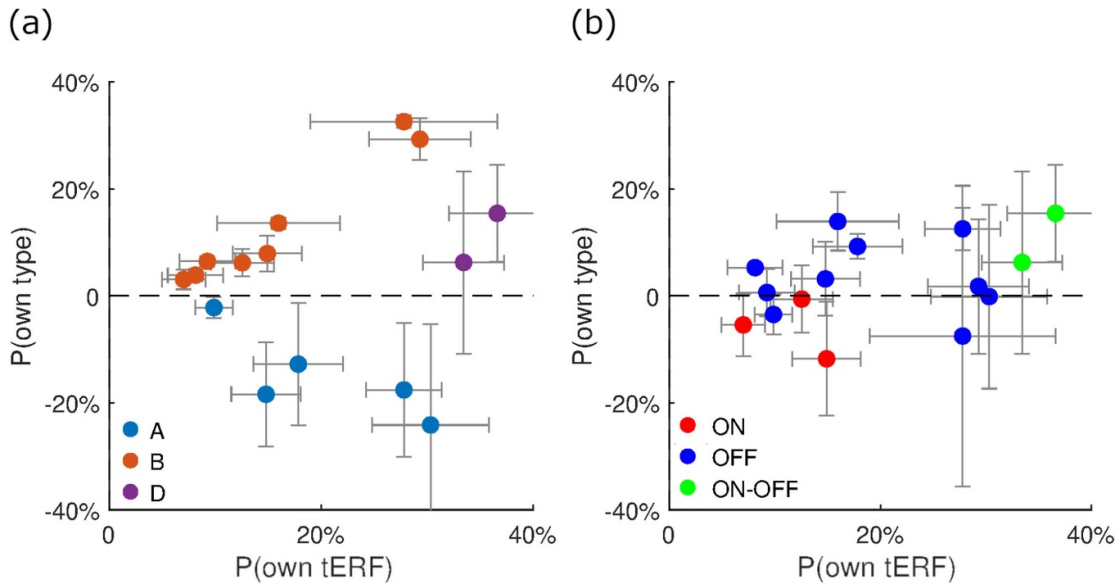


**Figure 9.** Population analysis of activation preference from extracellular stimulation. All data were from LE rats. The analysis is based on a: RGC morphological types and (b) light response types. In each subplot, the activation preference was obtained according to equation (2) or (3). Colours indicate to which cell type (A, B and D, or ON, OFF and ON-OFF) each cell belongs. The dashed lines indicate the line of equality. Error bars represent SEM.

A-cells did. In comparison, 9 out of 15 (60%) cells preferred their own light response type (figure 9(b)). Surprisingly, none of the ON cells showed preferences for their own light response type. However, as the numbers of cells recorded for these cell types are small, it requires further study to confirm the different preferences between cell types. Note that all D-cells have ON-OFF light response, hence the D-cells in figure 9(a) have the same response probability in $x$ and $y$ axis as the ON-OFF cells in figure 9(b).

## 4. Discussion

RGCs are the target of electrical stimulation for retinal prostheses because they survive retinal degeneration and thus retain the capacity to send information to the brain via their axons in the optic nerve. Current retinal prostheses use electrodes that have sizes larger than individual RGC somas and stimulate all surrounding RGCs in the same manner, which limits the quality of vision restored in patients. Although stimulation strategies for preferential stimulation of RGCs are under development, most studies only target limited RGC types. For example, high frequency stimulation was found effective in selectively stimulating ON and OFF RGCs [6, 9, 10]. Using biphasic stimulation at 200 Hz, D1 cells in the morphologically and biophysically detailed models of rat retina could be selectively stimulated over A2 cells [30]. Im *et al* found that the network-mediated responses in ON and OFF rabbit brisk cells show difference to stimulation durations [31, 32] and frequencies [32]. The only demonstration of preferential stimulation of individual cells was done by Fan *et al* [11] in which the authors showed that a careful selection of stimulating currents could avoid the activation of neighbouring neurons, and the stimulation selectivity could be improved using a local return electrode. Our work presents a novel approach to preferentially stimulate individual RGCs using their own tERFs from direct electrical stimulation.

### 4.1. tERF characteristics

In this study, we reconstructed the tERFs of RGCs per their responses to white noise current stimulation delivered both intracellularly and extracellularly. The tERFs of RGCs have been previously studied with white noise stimulation by several groups, but all obtained via extracellular stimulation [7, 8, 12, 15, 17]. Sekhar *et al* [8] first studied tERFs from the network-mediated response of RGCs. In their work, they delivered subthreshold subretinal stimulation and obtained the receptive fields using STA analysis. Their work revealed distinct characteristics of tERFs in healthy retinas based on their light responses, and the tERFs of ON cells had a short latency and upward deflection while the tERFs of OFF cells showed a short latency and downward deflection. In another study, Hofling *et al* [12] reconstructed tERFs of RGCs stimulated epiretinally using both STA and maximum likelihood estimate analysis. According to the response latencies of these tERFs, the authors suggested that these tERFs resulted from a combination of bipolar cell and direct RGC activation.

We used the STC analysis to reconstruct the tERFs of the RGCs in this work. While the STA provides a single linear filter that can be used to estimate the nonlinearity of the neuron, the STC provides multiple filters along with their variance which are

useful, for example, to find suppressive components within the stimuli [18, 33]. After a significance hypothesis test, we found that all the RGCs had significant excitatory receptive fields, but no significant suppressive receptive fields were observed in any cells. The excitatory receptive fields from the STC analysis (the tERF, or filter corresponding to the highest variance) were qualitatively consistent with their STAs in magnitudes, shapes and directions (e.g. figure 1(f)).

To our knowledge, this work is the first study of tERFs of RGCs via intracellular stimulation. The intracellular tERFs of all RGCs showed a single upward deflection (figures 2 and 5), whereas the tERFs obtained through extracellular stimulation show opposite deflection (figure 8). In contrast to Sekhar *et al* [8] and Hofling *et al* [12], we did not observe any cells with notable upward deflections. As the response delays for all extracellular tERFs were within 5 ms, these tERFs are likely correlated to the neural responses from direct electrical stimulation [13]. The upward deflections observed in the two above-mentioned studies were likely a result of network mediated activation.

### 4.2. tERF and cell type correlation

In this study, we classified the rat RGCs according to their morphology as A–D cells. The terminology of RGC morphological types varies among different species [2]. For example, cells with large soma and dendritic fields are often called A cells in rat [34], but alpha cells in mouse [4] and cat [35], brisk transient cells in rabbit [36] and parasol cells in primate [37]. Cells with small soma and dendritic field are often called B cells in rat [34], beta cells in mouse [4] and cat [35], brisk sustained cells in rabbit [36], and midget cells in primate [37]. The correlation of morphological types and their function or physiological properties may vary among the species. For example, while the midget cells are known to be responsible for high-acuity vision, it is less clear about the function of beta cells [4].

To further understand the variability of tERFs between cell types, we studied the correlation between cell types and tERFs by performing a clustering analysis using a K-means algorithm. For intracellular data, our results indicate that A-cells were the most prominent in both healthy and degenerated retinas (figure 5). Over 70% of the A-cells belonged to the same cluster. As A cells have large sizes of somas and dendritic fields, we wanted to understand if the difference was due to the cell size. We did not observe clear correlation between soma or dendritic field sizes and the tERF parameters (data not shown). This result is in line with several experimental and modelling studies which suggested that soma and dendritic field sizes alone have minimal correlations with response thresholds of certain Alpha RGC types in mice, whereas the axon initial segment (AIS) length and the distribution of $Na_v1.6$ channels along the AISs exert stronger influence [38–42]. RGCs are known to have varying physiological and morphological properties depending on their cell types and their locations in the retina. For example, in mouse retina, different types of RGCs have different calcium channel distributions [43]. Their AIS lengths and distances away from the soma also vary depending on the cell types and locations [41, 42]. Further investigation is needed to fully understand the tERF variability observed in this study. Since A cells have tERFs different from other cell types, tERFs may be used to identify A cells when morphological reconstruction is difficult. These results also further demonstrated that the intrinsic biophysical properties and morphological properties of individual cells could influence their sensitivity to stimulation.

### 4.3. Difference between intracellular and extracellular stimulation

The clustering results from extracellular stimulation showed that the cells, in general, distributed evenly among clusters and no cell type had more than 60% of the cells within a single cluster (figure 8). The difference between intracellular and extracellular stimulation results may be partially due to the electrode placement. The AIS, which is located about 10 $\mu$m away from the RGC soma, was previously found to be the most excitable part of a cell [38]. During the extracellular stimulation experiments, for practical reasons, we had to place the extracellular electrodes approximately 50 $\mu$m from the soma, but the relative location between the electrode and the AIS was difficult to control accurately without losing the cell patch. On the other hand, the intracellular stimulation was injected via the patch clamping electrode that was attached to the soma. The electrode placement distance and location relative to the AISs in the extracellular stimulation is expected to have some impact on the shape of the tERFs. Thus, a further study where the position of the stimulating electrode can be controlled, relative to the AIS, might result in tERFs that preferentially excite cell types more accurately. This could be achieved by visualising the Alexa Fluor$^{TM}$ 488-filled cell and axons under confocal/two-photon microscopes while placing the extracellular electrodes.

Another potential difference between intracellular and extracellular stimulation is related to direct and indirect stimulations of the RGCs. RGCs can be directly activated by an electrical stimulus, where the response has a short latency of less than 5 ms after stimulation; or indirectly activated by the retinal network, where the stimulus activates several different classes of retinal neurons, which in turn, elicit synaptic spikes on the RGCs [44, 45]. Indirect RGC stimulation may take advantages of the natural signal processing in the retina [31, 32], although network remodelling can happen during degeneration

[46], making it less helpful when the degeneration is at an advanced stage.

The direct/indirect activation is unlikely the reason behind the differences observed between intracellular and extracellular stimulation in this work, as our analysis of extracellular data was performed exclusively on spikes resulting from direct activation. As shown in figures 5 and 8, all the tERFs obtained had a latency shorter than 5 ms. Additionally, the shape and duration of the recovered tERFs correspond to the strong, short pulses typically found to directly activate RGCs as opposed to the longer stimulus duration observed in indirect activation [31, 47]. The STC analysis was performed over a time window much longer than the resulting tERFs, and we did not observe a distinct waveform, other than noise, within approximately 100 ms prior to the spikes (see figures 1(f) and 4(a)), which is the typical latency for indirect activation [31]. This contrasts with the STA study by Ho *et al* [15] which found longer latency and duration waveforms for network-mediated activation of RGCs, however, their electrode placement was subretinal as opposed to our epiretinal protocol, hence closer to the bipolar cells than the RGCs. Additionally, Sekhar *et al* [7] used subthreshold stimulation levels, which we hypothesize could result in less direct activation RGC spikes when stimulating, and their analysis focused only on indirect activation. Another indication of direct activation is the deflection of the extracellular tERFs. We only found extracellular tERFs with a single downward deflection, but if network-mediated responses were involved, tERFs would show upward deflections [7, 8, 12]. This is evident in work by Sekhar *et al* [7], where tERFs of ON cells had upward deflection and the tERFs of OFF cells had downward deflection.

### 4.4. Preferential activation of RGCs

In this work, we compared the sensitivity of RGCs to tERFs recovered from different neurons. As expected, both the intracellular and extracellular stimulation thresholds were lower when the cells were stimulated with their own tERFs compared to the tERFs of other cells (figures 7 and 9). However, the degree of preference varies among cells and among stimulation protocols. For instance, with extracellular stimulation, the thresholds were on average 20% lower in response to their own tERFs than to other cells' tERFs, while with intracellular stimulation, it was close to 8% in LE rats. This result indicates that RGCs can be preferentially stimulated when using stimulation that take the form of their own tERFs. We hypothesized that the cells might also prefer the tERFs of their own cell types, compared to those from other cell types. From intracellular data in LE rats, we showed that over 70% of the cells preferred the tERFs from their own morphological types (figure 7). The ratios of cells that preferred their own light response types were over 60%. When the cells were stimulated extracellularly, over 60% of the cells showed preferences for their own morphological or light response types (figure 9). Interestingly, when stimulated extracellularly, none of the A-cells showed preferences to the tERFs obtained from the other A-cells. Similar results were also observed in ON cells; they did not like the tERFs from the other ON cells (6% preference to other types). These extracellular results were consistent with the intracellular results from LE rats, in which all of the A-cells and most ON cells (4 out of 6) did not prefer the tERFs from their own cell types. With extracellular stimulation, both B and D cells preferred a stimulus from tERFs of their own morphological type. Specifically, the threshold of B-cells in response to the tERFs of other B-cells was, in average, 13% lower than in response to tERFs of other morphological types. And the threshold of D-cells in response to tERFs of other D-cells was 11% lower than in response to tERFs of other morphological types (figure 9). The threshold differences are small in some cases, which might limit the effectiveness of targeting cell types to some extent.

### 4.5. Impact of retinal degeneration

The performance of retinal stimulation devices has been found to be reduced in degenerated retinas. For example, previous research showed that in degenerated retinas, the RGCs showed increased spontaneous activities, low field background oscillations and abnormal light-evoked spike rates [48–50]. During electrical stimulation, an elevated charge was found to be necessary for triggering action potentials, at least in a subset of RGCs following degeneration [51]. While the differences may be partly due to retinal remodelling, it is unclear whether there are changes in the intrinsic physiological properties of the RGCs. During intracellular stimulation, the impact of retinal networks on RGC behaviour is negligible. Therefore, the intracellular tERF largely represents the intrinsic properties of RGCs. We compared the parameters from tERFs obtained from healthy and degenerated rat retinas, and our results did not show significant differences between the tERFs from the two animal models. This suggests that in RCS rats at least, the intrinsic properties of RGCs remain similar after retinal degeneration. In addition, we did not observe obvious changes in morphological features such as soma and dendritic field sizes and shapes between healthy and degenerated RGCs. In this study, we used RCS rats between the age of 4 and 15 months. It was known that the RCS rats lose their outer nuclear layer and RGC light responses around 3 months after birth [23]. We were not able to record any light responses from the RGCs of RCS retinas. Several studies have investigated the effect of the retina degeneration progression on the RGCs. In a mouse model for retina degeneration (rd10), where cone photoreceptors were mostly gone by 60 days postnatal, Stasheff *et al* [50]

showed that the RGC spontaneous and electrically evoked spiking responses tend to remain unchanged after P60. Even though another study by Park *et al* [49] has indicated some changes in evoked the RGC spiking between 10 and 20 weeks old rd10 mice, they also found spontaneous spiking in the RGCs largely unchanged after 10 weeks. Under comparison, rd1 mice, which is a model for early onset, rapidly progressing photoreceptor degeneration, continues to show changes in RGC responses beyond the completion of photoreceptor loss [50]. The RCS rat model is similar to the rd10 mouse model in terms of the speed of degeneration, therefore we expect minimal changes in the RGC responses in rats aged between 4 and 15 months.

### 4.6. Limitations

Practically, this research suggests that a retinal prosthesis designed to work at a single cell resolution can have improved performance when stimulating using the cell's tERF. In the extracellular stimulation experiments, we placed the 100 $\mu$m diameter stimulating electrode epiretinally, about 50 $\mu$m away from the soma. We showed that the recorded RGCs could be preferentially stimulated using their own tERFs. This indicates that our strategy may be effective at targeting RGCs that have their somata within 50 $\mu$m of the stimulation electrode. While this work provided some evidence to support the feasibility of this proposed stimulation strategy, there are several limitations. First of all, existing retinal prostheses can only stimulate [2]. To implement the proposed strategy, we will need the next generation of retinal prostheses to be capable of electrical stimulation and have the ability to simultaneously record single-unit activities from the target RGCs. The development of such a device is currently challenging. However, high spatiotemporal resolution recording of RGCs has already been demonstrated both *in vitro* [52] and *in vivo* [53]. Of particular interest is the recent development of polymer-based microelectrode arrays that can have close contact between the electrodes and retina surface after implantation [53, 54]. Secondly, it is well-known that to safely stimulate neurons, charge-balanced tERFs should be used [55]. However, according to our results, the tERFs of RGCs have monophasic structures. Long-term stimulation using monophasic tERFs may be dangerous to both the electrodes and surrounding neurons. A potential solution is to modify the stimulation tERFs by adding an opposite phase to offset the charge. However, it is necessary to reassess the efficacy of the stimulation strategy using modified tERFs. Third, to record from the cells, we performed whole-cell patch clamp recording. Although current retinal prosthetic devices do not allow intracellular recording, whole-cell patch clamp enabled us to retrieve the cell morphology by injecting fluorescent dye into the cell for post-recording imaging. In addition, the whole-cell configuration also enabled us to identify the light-response types of the RGCs in the degenerated retina, as they have lost their light responses. However, we acknowledge that future studies will need to repeat this work by recording the RGCs responses extracellularly in both healthy and degenerated retinas. Fourth, the activation of axon bundles is one major limitation in the spatial resolution from epiretinal stimulation [56–59]. When the axon bundles are activated, RGCs with somata far away from the stimulation electrodes may be stimulated, leading to patients reporting elongated phosphenes [58]. The strategy proposed here is promising for addressing the issue, as the tERFs are expected to be different for the target RGCs and the axon bundles. However, we were unable to study the impact of axon bundle activation in this study as we recorded from single neurons using whole-cell patch clamping. Other recording techniques such as calcium imaging [56, 57] and multielectrode array recording [59] will be required to study the spatial distribution of RGC activation. The small threshold differences observed in some cells represent the last limitation in the application of the proposed strategy.

## 5. Conclusion

This work proposes a stimulation strategy for preferential stimulation of individual RGCs for retinal prostheses. This strategy is implemented by first reconstructing the tERFs of RGCs according to their response to Gaussian white noise current stimulation, and then stimulating the target cells using their own tERFs. In this work, we demonstrated the strategy through both intracellular and extracellular stimulation. By comparing the tERFs reconstructed from RGCs, we found some correlation between A-cells and their intracellular tERFs, but the correlation was less obvious between the cell types and their extracellular tERFs. Our results also showed that the RGCs had lower activation thresholds when stimulated using their own tERFs, and about 60%–70% of the cells also preferred the tERFs from other cells within their own morphological or light response types, as opposed to tERFs from other cell types. Such a stimulation strategy, in combination with a device that is capable of both neural stimulation and recording, can be used to target individual neurons around a single stimulating electrode.

## Data availability statement

The data that support the findings of this study are available upon reasonable request from the authors.

## Acknowledgment

AS acknowledges the support of Consejo Nacional de Ciencia y Tecnologia (CONACYT), Mexico,

Scholarship No. 399077. WT was supported by a Linkage Grant (LP180100638) and a DECRA Fellowship (DE220100302) from the Australian Research Council.

## ORCID iDs

Molis Yunzab https://orcid.org/0000-0003-3642-0077
Artemio Soto-Breceda https://orcid.org/0000-0002-7162-2590
Wei Tong https://orcid.org/0000-0002-3725-2928

## References

[1] Goetz G A and Palanker D V 2016 Electronic approaches to restoration of sight *Rep. Prog. Phys.* **79** 096701
[2] Tong W, Meffin H, Garrett D J and Ibbotson M R 2020 Stimulation strategies for improving the resolution of retinal prostheses *Front. Neurosci.* **14** 262
[3] Humayun M S, Prince M, de Juan E, Barron Y, Moskowitz M, Klock I B and Milam A H 1999 Morphometric analysis of the extramacular retina from postmortem eyes with retinitis pigmentosa *Invest. Ophthalmol. Vis. Sci.* **40** 143–8 (available at: https://iovs.arvojournals.org/article.aspx?articleid=2162046)
[4] Sanes J R and Masland R H 2015 The types of retinal ganglion cells: current status and implications for neuronal classification *Annu. Rev. Neurosci.* **38** 221–46
[5] Yang C Y, Tsai D, Guo T, Dokos S, Suaning G J, Morley J W and Lovell N H 2018 Differential electrical responses in retinal ganglion cell subtypes: effects of synaptic blockade and stimulating electrode location *J. Neural Eng.* **15** 046020
[6] Guo T, Yang C Y, Tsai D, Muralidharan M, Suaning G J, Morley J W, Dokos S and Lovell N H 2018 Closed-loop efficient searching of optimal electrical stimulation parameters for preferential excitation of retinal ganglion cells *Front. Neurosci.* **12** 168
[7] Sekhar S, Jalligampala A, Zrenner E and Rathbun D 2016 Tickling the retina: integration of subthreshold electrical pulses can activate retinal neurons *J. Neural Eng.* **13** 046004
[8] Sekhar S, Jalligampala A, Zrenner E and Rathbun D 2017 Correspondence between visual and electrical input filters of ON and OFF mouse retinal ganglion cells *J. Neural Eng.* **14** 046017
[9] Twyford P, Cai C and Fried S 2014 Differential responses to high-frequency electrical stimulation in ON and OFF retinal ganglion cells *J. Neural Eng.* **11** 025001
[10] Muralidharan M, Guo T, Shivdasani M N, Tsai D, Fried S, Li L, Dokos S, Morley J W and Lovell N H 2020 Neural activity of functionally different retinal ganglion cells can be robustly modulated by high-rate electrical pulse trains *J. Neural Eng.* **17** 045013
[11] Fan V H, Grosberg L E, Madugula S S, Hottowy P, Dabrowski W, Sher A, Litke A M and Chichilnisky E 2019 Epiretinal stimulation with local returns enhances selectivity at cellular resolution *J. Neural Eng.* **16** 025001
[12] Höfling L, Oesterle J, Berens P and Zeck G 2020 Probing and predicting ganglion cell responses to smooth electrical stimulation in healthy and blind mouse retina *Sci. Rep.* **10** 1–20
[13] Maturana M I, Apollo N V, Hadjinicolaou A E, Garrett D J, Cloherty S L, Kameneva T, Grayden D B, Ibbotson M R, Meffin H and Pillow J W 2016 A simple and accurate model to predict responses to multi-electrode stimulation in the retina *PLoS Comput. Biol.* **12** e1004849
[14] Maturana M I, Apollo N V, Garrett D J, Kameneva T, Cloherty S L, Grayden D B, Burkitt A N, Ibbotson M R, Meffin H and Fine I 2018 Electrical receptive fields of retinal ganglion cells: influence of presynaptic neurons *PLoS Comput. Biol.* **14** e1005997
[15] Ho E, Smith R, Goetz G, Lei X, Galambos L, Kamins T I, Harris J, Mathieson K, Palanker D and Sher A 2018 Spatiotemporal characteristics of retinal response to network-mediated photovoltaic stimulation *J. Neurophysiol.* **119** 389–400
[16] Rathbun D, Ghorbani N, Shabani H, Zrenner E and Hosseinzadeh Z 2018 Spike-triggered average electrical stimuli as input filters for bionic vision—a perspective *J. Neural Eng.* **15** 063002
[17] Sekhar S, Ramesh P, Bassetto G, Zrenner E, Macke J H and Rathbun D L 2020 Characterizing retinal ganglion cell responses to electrical stimulation using generalized linear models *Front. Neurosci.* **14** 378
[18] Chichilnisky E 2001 A simple white noise analysis of neuronal light responses *Netw. Comput. Neural Syst.* **12** 199–213
[19] Tong W, Stamp M, Apollo N V, Ganesan K, Meffin H, Prawer S, Garrett D J and Ibbotson M R 2019 Improved visual acuity using a retinal implant and an optimized stimulation strategy *J. Neural Eng.* **17** 016018
[20] Zollo L *et al* 2019 Restoring tactile sensations via neural interfaces for real-time force-and-slippage closed-loop control of bionic hands *Sci. Robot.* **4** eaau9924
[21] Willett F R, Avansino D T, Hochberg L R, Henderson J M and Shenoy K V 2021 High-performance brain-to-text communication via handwriting *Nature* **593** 249–54
[22] Chen X, Wang F, Fernandez E and Roelfsema P R 2020 Shape perception via a high-channel-count neuroprosthesis in monkey visual cortex *Science* **370** 1191–6
[23] Strauss O, Stumpff F, Mergler S, Wienrich M and Wiederholt M 1998 The Royal College of Surgeons rat: an animal model for inherited retinal degeneration with a still unknown genetic defect *Cells Tissues Organs* **162** 101–11
[24] Soto-Breceda A, Kameneva T, Meffin H, Maturana M and Ibbotson M 2018 Irregularly timed electrical pulses reduce adaptation of retinal ganglion cells *J. Neural Eng.* **15** 056017
[25] Kiyatkin E A 2019 Brain temperature and its role in physiology and pathophysiology: lessons from 20 years of thermorecording *Temperature* **6** 271–333
[26] Gotoh M, Nagasaka K, Nakata M, Takashima I and Yamamoto S 2020 Brain temperature alters contributions of excitatory and inhibitory inputs to evoked field potentials in the rat frontal cortex *Front. Cell Neurosci.* **14** 593027
[27] Schindelin J *et al* 2012 Fiji: an open-source platform for biological-image analysis *Nat. Methods* **9** 676–82
[28] Lloyd S 1982 Least squares quantization in PCM *IEEE Trans. Inf. Theory* **28** 129–37
[29] MacQueen J 1967 Some methods for classification and analysis of multivariate observations pp 281–97 (available at: https://projecteuclid.org/ebooks/berkeley-symposium-on-mathematical-statistics-and-probability/Some-methods-for-classification-and-analysis-of-multivariate-observations/chapter/Some-methods-for-classification-and-analysis-of-multivariate-observations/bsmsp/1200512992)
[30] Paknahad J, Loizos K, Yue L, Humayun M S and Lazzi G 2021 Color and cellular selectivity of retinal ganglion cell subtypes through frequency modulation of electrical stimulation *Sci. Rep.* **11** 1–13
[31] Im M, Werginz P and Fried S I 2018 Electric stimulus duration alters network-mediated responses depending on retinal ganglion cell type *J. Neural Eng.* **15** 036010
[32] Im M and Fried S I 2016 Temporal properties of network-mediated responses to repetitive stimuli are dependent upon retinal ganglion cell type *J. Neural Eng.* **13** 025002
[33] Schwartz O, Pillow J W, Rust N C and Simoncelli E P 2006 Spike-triggered neural characterization *J. Vis.* **6** 13
[34] Wong R C S, Cloherty S L, Ibbotson M R and O'Brien B J 2012 Intrinsic physiological properties of rat retinal ganglion cells with a comparative analysis *J. Neurophysiol.* **108** 2008–23

[35] O'Brien B J, Isayama T, Richardson R and Berson D M 2002 Intrinsic physiological properties of cat retinal ganglion cells *J. Physiol.* **538** 787–802
[36] Amthor F R, Takahashi E S and Oyster C W 1989 Morphologies of rabbit retinal ganglion cells with concentric receptive fields *J. Comp. Neurol.* **280** 72–96
[37] Dacey D M and Petersen M R 1992 Dendritic field size and morphology of midget and parasol ganglion cells of the human retina *Proc. Natl Acad. Sci.* **89** 9666–70
[38] Fried S I, Lasker A C, Desai N J, Eddington D K and Rizzo J F 3rd 2009 Axonal sodium-channel bands shape the response to electric stimulation in retinal ganglion cells *J. Neurophysiol.* **101** 1972–87
[39] Werginz P, Raghuram V and Fried S I 2020 The relationship between morphological properties and thresholds to extracellular electric stimulation in $\alpha$ RGCs *J. Neural Eng.* **17** 045015
[40] Jeng J, Tang S, Molnar A, Desai N and Fried S 2011 The sodium channel band shapes the response to electric stimulation in retinal ganglion cells *J. Neural Eng.* **8** 036022
[41] Werginz P, Raghuram V and Fried S I 2020 Tailoring of the axon initial segment shapes the conversion of synaptic inputs into spiking output in OFF-$\alpha$ T retinal ganglion cells *Sci. Adv.* **6** eabb6642
[42] Raghuram V, Werginz P and Fried S I 2019 Scaling of the AIS and somatodendritic compartments in $\alpha$ S RGCs *Front. Cell Neurosci.* **13** 436
[43] Margolis D J, Gartland A J, Euler T and Detwiler P B 2010 Dendritic calcium signaling in ON and OFF mouse retinal ganglion cells *J. Neurosci.* **30** 7127–38
[44] Fried S I, Hsueh H A and Werblin F S 2006 A method for generating precise temporal patterns of retinal spiking using prosthetic stimulation *J. Neurophysiol.* **95** 970–8
[45] Medeiros N E and Curcio C A 2001 Preservation of ganglion cell layer neurons in age-related macular degeneration *Invest. Ophthalmol. Vis. Sci.* **42** 795–803
[46] Jones B W and Marc R E 2005 Retinal remodeling during retinal degeneration *Exp. Eye Res.* **81** 123–37
[47] Jensen R J and Rizzo J F III 2008 Activation of retinal ganglion cells in wild-type and rd1 mice through electrical stimulation of the retinal neural network *Vis. Res.* **48** 1562–8
[48] Margolis D J, Newkirk G, Euler T and Detwiler P B 2008 Functional stability of retinal ganglion cells after degeneration-induced changes in synaptic input *J. Neurosci.* **28** 6526–36
[49] Park D, Senok S and Goo Y-S 2015 Degeneration stage-specific response pattern of retinal ganglion cell spikes in rd10 mouse retina pp 3351–4
[50] Stasheff S F, Shankar M and Andrews M P 2011 Developmental time course distinguishes changes in spontaneous and light-evoked retinal ganglion cell activity in rd1 and rd10 mice *J. Neurophysiol.* **105** 3002–9
[51] Cho A, Ratliff C, Sampath A and Weiland J 2016 Changes in ganglion cell physiology during retinal degeneration influence excitability by prosthetic electrodes *J. Neural Eng.* **13** 025001
[52] Fiscella M, Farrow K, Jones I L, Jäckel D, Müller J, Frey U, Bakkum D J, Hantz P, Roska B and Hierlemann A 2012 Recording from defined populations of retinal ganglion cells using a high-density CMOS-integrated microelectrode array with real-time switchable electrode selection *J. Neurosci. Methods* **211** 103–13
[53] Hong G, Fu T-M, Qiao M, Viveros R D, Yang X, Zhou T, Lee J M, Park H-G, Sanes J R and Lieber C M 2018 A method for single-neuron chronic recording from the retina in awake mice *Science* **360** 1447–51
[54] Hong G and Lieber C M 2019 Novel electrode technologies for neural recordings *Nat. Rev. Neurosci.* **20** 330–45
[55] Cogan S F 2008 Neural stimulation and recording electrodes *Annu. Rev. Biomed. Eng.* **10** 275–309
[56] Tong W, Hejazi M, Garrett D J, Esler T, Prawer S, Meffin H and Ibbotson M R 2020 Minimizing axon bundle activation of retinal ganglion cells with oriented rectangular electrodes *J. Neural Eng.* **17** 036016
[57] Weitz A C, Nanduri D, Behrend M R, Gonzalez-Calle A, Greenberg R J, Humayun M S, Chow R H and Weiland J D 2015 Improving the spatial resolution of epiretinal implants by increasing stimulus pulse duration *Sci. Trans. Med.* **7** 318ra203
[58] Beyeler M, Nanduri D, Weiland J D, Rokem A, Boynton G M and Fine I 2019 A model of ganglion axon pathways accounts for percepts elicited by retinal implants *Sci. Rep.* **9** 1–16
[59] Grosberg L E *et al* 2017 Activation of ganglion cells and axon bundles using epiretinal electrical stimulation *J. Neurophysiol.* **118** 1457–71